Fizika Nizkikh Temperatur, 2003, v. 29, Nos. 9/10, p. 1081–1092

Prompt and delayed secondary excitons in rare gas solids

M. Kirm[1], V. Kisand[2], E. Sombrowski[3], B. Steeg[3], S. Vielhauer[1], and G. Zimmerer[1]

[1] *Institut für Experimentalphysik, University of Hamburg, 149 Luruper Chaussee, Hamburg D–22761, Germany*
E-mail: Georg.Zimmerer@desy.de

[2] *Institute of Physics, University of Tartu, 142 Riia, Tartu 51014, Estonia*

[3] *Deutsches Elektronensynchrotron DESY, 85 Notkestrasse, Hamburg 22607, Germany*

Direct and indirect creation of excitons in rare gas solids has been investigated with reflectivity and luminescence spectroscopy. For the heavy rare gas solids Kr and Xe, new and more reliable exciton parameters have been deduced. With time-resolved luminescence spectroscopy, fast and delayed secondary-exciton creation has been established and separated. Thermalization of photocarriers and their delayed recombination have been analyzed, including a first attempt to investigate the influence of excitation density on the carrier dynamics. The existence of excitonic side bands of ionization limits E_i (either band gap or inner-shell ionization limits) in prompt secondary exciton creation has been established. The threshold energies of these side bands are given by $E_{\rm th} \approx E_i + nE_{\rm ex}$ (n is integer, $E_{\rm ex}$ is exciton energy). The side bands are ascribed to the formation of electronic polaron complexes, superimposed to inelastic scattering of photoelectrons.

PACS: 71.35.Cc, 72.20.Jv, **78.47.+p**, 78.55.Hx

Introduction

At the onset of optical excitation of rare gas solids (RGS) in the vacuum ultraviolet spectral range, pronounced absorption lines are found. They arise from the creation of bound pairs of valence holes and conduction electrons in the centre of the Brillouin zone (Γ-point) and can be arranged in two series, $\Gamma(3/2)$ $\Gamma(3/2)$ and $\Gamma(1/2)$, depending on the total angular momentum $j = 3/2$ or $j = 1/2$ of the hole. These excitations have been subject of numerous investigations because rare gas solids are model systems for excitons in insulators [1–4]. It is not the purpose of this article to review the field, but to describe some special aspects of exciton creation which have been investigated in recent years. We have to discriminate between *direct* and *indirect* creation of excitons. *Direct* creation is achieved, e.g., by optical excitation with an appropriate photon energy, $E_{\rm ph} = E_{\rm ex}$ ($E_{\rm ph}$ is photon energy of excitation; $E_{\rm ex}$ is exciton energy). Some aspects of direct creation will be discussed in Sec. 2, because they are necessary for a better understanding of the *indirect* creation processes. Indirect exciton creation arises from (i) recombination of electron-hole pairs, (ii) inelastic scattering of photoelectrons, and (iii) excitonic side bands of valence or inner-shell excitations.

All experimental results have been obtained with synchrotron radiation (SR) excitation at the Hamburger Synchrotronstrahlungslabor HASYLAB at DESY, Hamburg. Two beamlines have been used, namely beamline «I» with the set-up SUPERLUMI (normal incidence; range of excitation ≤ 40 eV), and beamline «BW3» (grazing incidence; range of excitation 30 eV ≤ $h\nu$ ≤ 1000 eV). As the main part of the present paper deals with time-resolved data, some details are given here. SR at HASYLAB consists of pulses with FWHM ≅ 150 ps, at a repetition rate between 5 and 1 MHz, depending on the mode of operation. For more details, we refer to the original papers cited. If necessary, in a few cases, more details are given in the text.

1. Direct exciton creation

1.1. Reflectivity and new evaluation of exciton parameters

Excitons in rare gas solids are ascribed to the «intermediate» type [5] which means that the energetic

© M. Kirm, V. Kisand, E. Sombrowski, B. Steeg, S. Vielhauer, and G. Zimmerer, 2003

positions of the lines corresponding to the main quantum numbers $n > 1$ are well described by the Wannier formula,

$$E_{nj} = E_j - \frac{B_j}{n^2} \qquad (1)$$

(E_{nj} is energy of exciton with main quantum number n; E_j is ionization limit of the exciton series; $E_{3/2} = E_g$, E_g is band gap energy; B_j is binding energy of the exciton series). According to former measurements, however, the members with n = 1 yield more or less pronounced deviations from the Wannier formula (see, e.g., [3]). The reflectivity curves of Kr and Xe have been carefully re-measured in the excitonic range because the preparation of polycrystalline [6,7] or even monocrystalline rare gas samples [8] with high structural quality has been developed. Moreover, contrary to the early investigations, now a more precise determination of the energies of $n = 1$ excitons from photoluminescence (the so-called free-exciton (FE) lines) is possible (see Sec. 1.2). As an example, in Fig. 1, the reflectivity of Kr is presented [9] (for Xe see Ref. 10). Five members of the $\Gamma(3/2)$ series are observed. The $n = 1$ band clearly displays an exciton-polariton nature. In the case of Xe, a quantitative analysis has been performed in terms of the exciton-polariton model [8], showing that the deduced energy of the transverse exciton agrees with the energy of the FE line in photoluminescence. In the case of Kr, a line-shape analysis of the reflectivity curve in terms of the exciton-polariton model has not been carried out because only the energy of the transverse exciton, which was taken from luminescence, is required for the following conclusions.

In Fig. 2, the energies of the Kr excitons are plotted as a function of $1/n^2$. All energies, including $n = 1$,

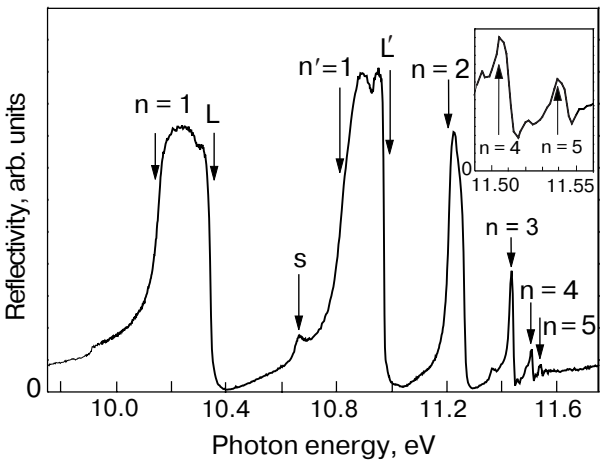

Fig. 1. Reflectivity of solid Kr, measured at T = 6 K with a resolution interval $\Delta\lambda = 0.6$ Å [9]. The inset shows the range of n = 4 and n = 5 excitons in an enlarged scale.

obey the Wannier formula with high accuracy. The same is true for Xe [10]. In so far, the former discussion of corrections of the $n = 1$ value (see, e.g., references given in Refs. 1–5) is obsolete in the case of Kr and Xe. This, however, does not mean that the model of the intermediate exciton is ruled out in general. In the case of the light rare gas solids Ar and Ne the $n = 1$ value indeed deviates from the Wannier formula. Interestingly, in the light rare gas solids, the excitons are unstable against exciton-lattice interaction, whereas they are metastable in the case of the heavier rare gas solids. Consequently, no FE lines but mainly the emission of self-trapped excitons (STE) show up in the luminescence spectra of Ar and Ne, whereas both types of luminescence coexist in the case of Xe and Kr. In Table 1, the exciton parameters deduced from the new reflectivity curves are presented and compared with former results.

Table 1

Exciton parameters of solid Kr and Xe at T = 6 K

Parameter	Unit	Value of the parameter	
		Kr	Xe
Binding energy	eV	(1.45±0.02)[a]	(0.903±0.036)[d]
		1.53[b]	1.02[b]
		1.73[c]	0.86[c]
Band gap	eV	(11.59±0.01)[a]	(9.298±0.005)[d]
		11.61[b]	9.33[b]
		11.67[c]	9.28[c]
Reduced mass	m_0	(0.377±0.005)[a]	(0.327±0.005)[d]
		0.40[b]	0.37[b]
		0.41 (with $\varepsilon_r = 1.80$)[c]	0.31 (with $\varepsilon_r = 2.23$)[c]

Comment: [a]Ref. 9; [b]Ref. 3; [c]Ref. 11; [d]Refs. 10, 30.

1.2. Radiative exciton decay

Following photon excitation of valence excitons of Kr and Xe, luminescence spectra are observed which yield (i) narrow lines originating from the free $n = 1$ (transverse) exciton and (ii) broad, Stokes shifted bands originating from self-trapped excitons. In Fig. 3, Kr results are given [9,12] (Xe results are published, e.g., in Ref. 13). The Kr results are of special importance because the samples were nearly free from Xe impurities which efficiently quench the Kr FE line and which also modify the STE bands as a consequence of the luminescence of heteronuclear Kr–Xe* centres [9].

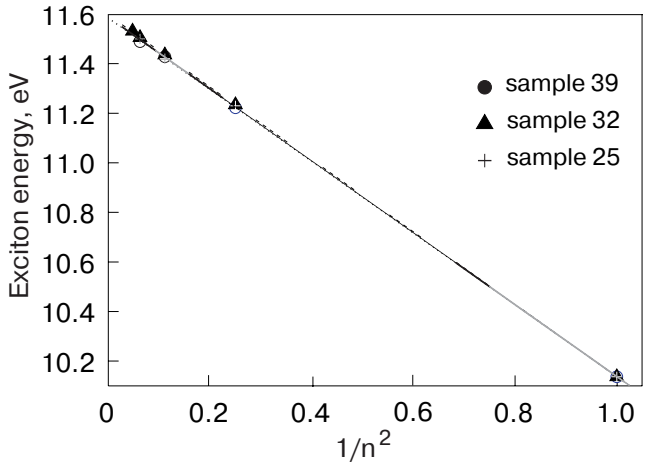

Fig. 2. Plot of exciton energies of the $\Gamma(3/2)$ series of solid Kr, measured at T = 6 K, as a function of $1/n^2$ (n is exciton quantum number) [9].

The decay curves in Fig. 3 display the decay of the FE line and the decay of the STE emission. The decay of the FE line is rather fast and nonexponential. For Xe, the details have been discussed in Ref. 13. The STE luminescence decay includes two components, one in the ns range originating from the singlet state of the STE, and another one in the μs range originating from the triplet state, showing up in the figure as a flat background. An analysis of the fast component shows that it displays a cascade behavior involving the decay of the FE line and the lifetime of the STE singlet state [14].

These remarks on the radiative decay of free excitons have been included because the central part of the present paper will deal with *modifications* in the case of indirect exciton creation.

2. Secondary excitons following valence excitations

2.1. Decay curves following near band-gap excitation

2.1.1. Xenon and krypton. The decay curves of the FE line observed under direct excitation are nonexponential with an approximate decay rate of the order of some 10^8 s^{-1} and a rise time < 100 ps (experimental time resolution) [12,13]. The situation changes as soon as the photon energy of excitation exceeds the band-gap energy. Then, as a result of the primary excitation, free electron-hole pairs are created. Nevertheless, the FE line still shows up with nearly the same intensity as under direct excitation of excitons. It is therefore obvious that recombination of electrons and holes into *free* excitons occurs. The decay curves, however, change dramatically as is shown for Kr [12] and Xe [15] in Figs. 4 and 5. The parameter of the curves is the excess energy, $E_{excess} = E_{\rm ph} - E_g$. It is the sum of the kinetic energies of both carriers involved. With increasing excess energy, the cascade-type shape gets more and more pronounced. Apart from the spike near to time zero, the whole luminescence intensity is delayed compared to the decay of directly excited excitons (for comparison, a directly excited curve is included in Fig. 5). This delay arises from a convolution of thermalization of the carriers and their recombina-

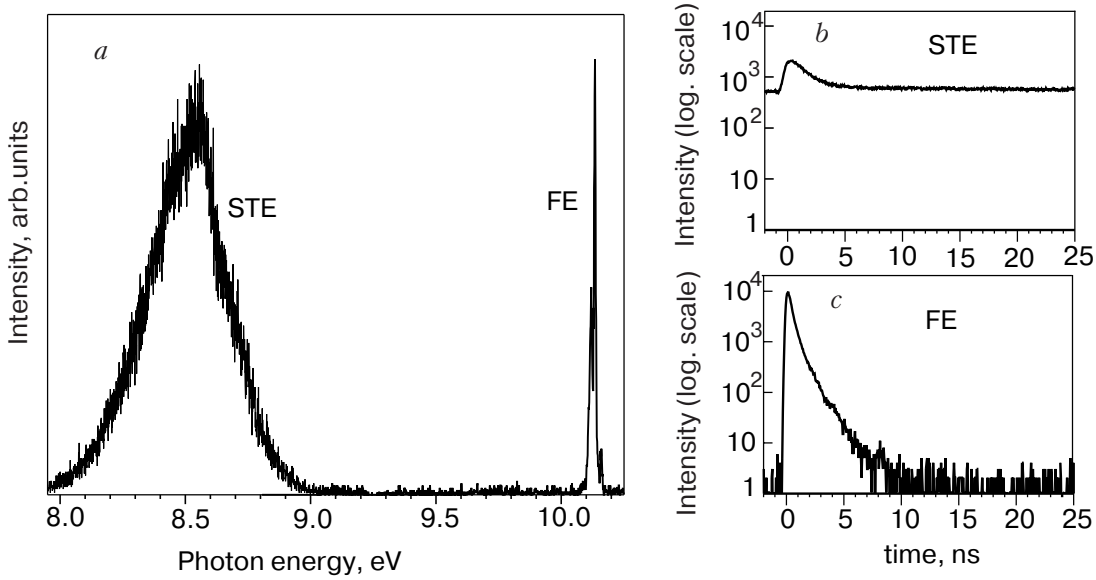

Fig. 3. (*a*) Luminescence of nearly Xe-free solid Kr, excited by 10.42 eV photons at T = 6 K and measured with a resolution interval $\Delta\lambda$ = 1.2 Å. (*b*) Decay curve of STE luminescence (measured at 8.55 eV), and (*c*) decay curve of FE luminescence (measured at 10.14 eV) of the same sample. Both decay curves were obtained with a resolution interval $\Delta\lambda$ = 9 Å at 6 K under excitation at 10.42 eV [12].

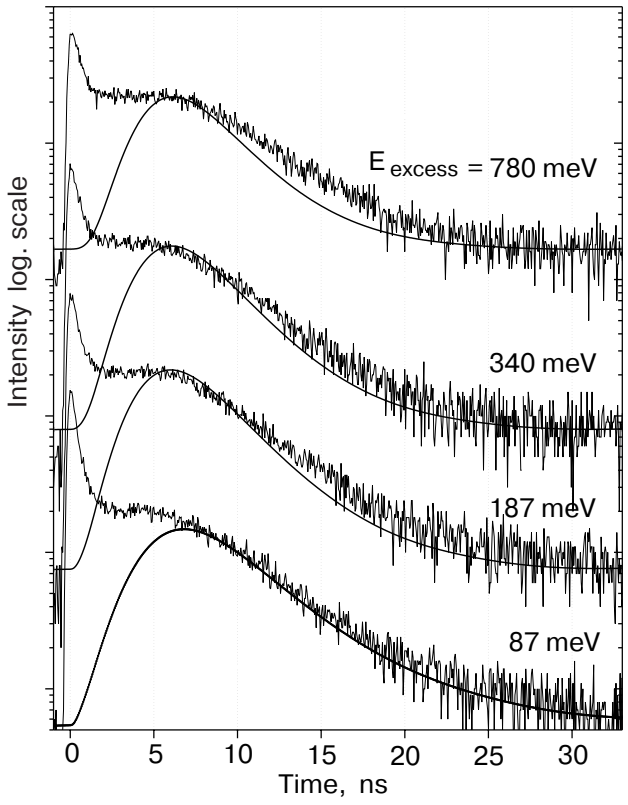

Fig. 4. FE decay curves of Kr, measured at T = 6 K, together with fitting results (full lines) for the delayed part [16]. Resolution intervals in excitation 3.5 Å and in emission 8 Å. The parameter of the curves is the excess energy.

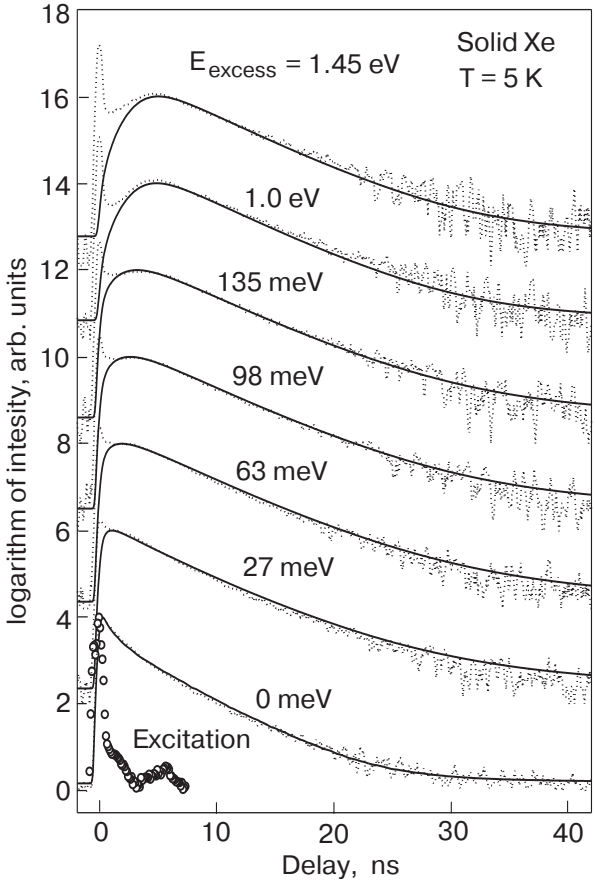

Fig. 5. FE decay curves of Xe, measured at T = 5 K, together with fitting results (full curves) for the delayed part [15]. The parameter of the curves is the excess energy. For comparison, an «apparatus function» (convolution of an excitation pulse with the response of the detector and the electronics) is included (open circles).

tion. Here, a special aspect of rare gas solids comes into play: the simple fcc lattice of the rare gas solids allows only for acoustical phonons which slows down thermalization of carriers, compared to, e.g., alkali halides. It turns out that the bottleneck of recombination is the thermalization process because the recombination cross section is a sensitive function of the velocity of the carriers [15].

The curves in Figs. 4 and 5 show also spikes at $t \approx 0$. They are ascribed to experimental artefacts. The monochromators used are single-pass instruments; therefore, a «white» background of VUV radiation (primary monochromator $\approx 10^{-3}$, secondary monochromator $\approx 10^{-2}$) is unavoidable. The background shows up at $t \approx 0$ as scattered light or even leads to direct excitation of excitons, although the photon energies chosen by the monochromator settings do not allow it.

The shape of the delayed FE luminescence was used to analyze the recombination dynamics of the photo carriers [15]. The full curves in Figs. 4 and 5 are results of model calculations in which the carrier dynamics have been treated in the following way [15,16]. The starting point is an initial mean kinetic energy of the carriers,

$$E_{0e,h} = \frac{m_{h,e}}{m_e + m_h} E_{\text{excess}} \qquad (2)$$

(the excess energy is shared among the carriers according to the effective masses m_e, and m_h), and a density of electrons and holes, $n_{e,0} = n_{h,0}$, which has been established due to the nearly δ-like photo-excitation. Assuming the carriers achieve a Maxwellian distribution of temperatures T_e and T_h, the energy loss of electrons, e, and holes, h, due to scattering on acoustical phonons, is described by [17]

$$\left\langle \frac{dE_{e,h}}{dt} \right\rangle_{\text{ac}} = -\frac{8\sqrt{2}E_d^2 m_{e,h}^{5/2}}{\pi^{3/2}\hbar^4\rho}(kT_{e,h})^{3/2}\left(\frac{T_{e,h} - T_L}{T_{e,h}}\right) \qquad (3)$$

with deformation potential E_d, effective masses m_e, and m_h, mass density ρ, lattice temperature T_L, and Boltzmann and Planck constants, k and $\hbar$. For RGS, $m_h >> m_e$, therefore the holes relax much faster than

the electrons (note the factor $m_{e,h}^{5/2}$ in the nominator of equation (3)). For that reason, we assume $T_h = T_L$.

For $t > 0$, the evolution of the carrier densities due to exciton formation and the exciton density, $n_{\rm ex}$, are described by the following rate equations

$$\frac{dn_{e,h}}{dt} = -\sigma(T_e) n_e n_h v_{\rm rel}(T_e) - \frac{n_{e,h}}{\tau_{nr}} \quad \text{and}$$

$$\frac{dn_{\rm ex}}{dt} = \sigma(T_e) n_e n_h v_{\rm rel}(T_e) - R(t) \qquad (4)$$

with a temperature dependent cross-section $\sigma(T_e)$, and relative velocity $v_{\rm rel}(T_e)$. The term $n_{e,h}/\tau_{nr}$ describes additional nonradiative carrier losses, e.g., at the surface. The decay of the exciton itself is described by the decay term $R(t)$, for which *experimental FE decay curves following direct photo-excitation of the excitons* measured at the same sample were used. For $\sigma(T_e)$, we use the formula given by Reimand et al. [15]*,

$$\sigma(T_e) = \frac{1}{(4\pi)^3} \frac{16\sqrt{2}e^6 E_d^2 m_e^{5/2}}{3\sqrt{3\pi}\hbar^4 c_s \rho (\varepsilon_0 \varepsilon_r)^3} \sqrt{\frac{m_e}{m_h}} \frac{1}{\sqrt{kT_L}(kT_e)^2} \qquad (5)$$

which is a modification of the formula given by Avakumov et al. [19] for $T_e \neq T_h$ (e is electron charge, c_s is sound velocity, $\varepsilon_0\varepsilon_r$ is dielectric permeability).

In the case of Xe, values for c_s, ρ, ε_r, m_h, and E_d were taken from the literature [1–4]. T_L was measured. Moreover, the sample quality was sufficiently good to neglect the nonradiative term in the kinetic equations. Then the only free adjustable parameter in the calculations was the initial density. A hidden approximation is the definition of an electron temperature of the relaxing system via $E = (3/2)\, kT_e$ (E is mean value of kinetic energy).

For Xe, the fits are quite acceptable. Nevertheless, the result has to be taken with care for the following reason. Among the parameters taken from the literature there are some which are known with high accuracy (c_s, ρ, ε_r) and others which are rather uncertain (m_e, m_h, and E_d). Concerning the effective masses, another difficulty has to be mentioned. In the model, isotropic parabolic bands are assumed, whereas the band structure of Xe and Kr is anisotropic. Moreover, the excess energies in the experiment extend to large values where the parabolic approximation breaks down. Therefore it is questionable to use the data for a deduction of more reliable values of, e.g., the mass or the deformation potential.

In the case of Kr, the model was modified in the following way. The term $E_d^2 m_e^{5/2}$ in the nominator of equation (5) is the most important factor. It is connected with the low field mobility according to [17,20]

$$\mu_0 = \frac{2}{3} \frac{\sqrt{2\pi} e \hbar^4 \rho v_l^2}{E_d^2 m_e^{5/2} (k_B T_L) \sqrt{k_B T_e}} . \qquad (6)$$

In the case of the low-field mobility, $T_L \approx T_e$, and ρv_l^2 is sufficiently well known (v_l is longitudinal sound velocity). Therefore, $E_d^2 m_e^{5/2}$ was calculated from the mobility measurements of Miller et al. [21]. In other words, using an experimental result, the most uncertain parameters were eliminated**. The Kr fits were obtained in this way. Although they are not as good as for the case of Xe, they are more satisfactory because the number of parameters has been decreased. The parameters of the fits are collected in Table 2.

The values of the initial carrier densities are by far much lower than those estimated from the photon flux and from the value of the absorption coefficient at the respective photon energy of excitation [15] for the following reasons. The initial density is the density after redistribution of the carriers via Coulomb scattering. During this first stage of relaxation, carrier diffusion decreases the density. Here, the geometry of excitation comes into play. The size of the spot at the sample surface is about 0.3×4 mm^2. The penetration depth of light is of the order of a few 100 Å. On the other side, it was shown that the scattering length of excitons is of the order of 1000 Å [13]. The scattering lengths of the carriers should be similar because both is scattering on acoustic phonons. With a scattering length exceeding the thickness of the initially excited volume by an order of magnitude, diffusion of the carriers into the bulk will rapidly decrease the carrier density.

This, however, raises the question why spatial diffusion has not been taken into account in the rate equations. Diffusion has been neglected there because the holes get self-trapped in rare gas solids. Then, the spatial diffusion of the electrons in a localized positively charged background is suppressed. It seems as if

* Compared to Ref. 15, a factor $1/(4\pi)^3$ was added so that this formula is valid for SI system. This was pointed out to us by A.N. Vasil'ev [18].

** This is not completely true because there is still the factor $\sqrt{m_e/m_h}$ in the equation. However, the errors introduced by this square root are much less than those introduced by $E_d^2 m_e^{5/2}$.

Table 2

The values of the parameters used for the fits of the time dependence of delayed FE luminescence in solid Kr and Xe shown in Figs. 4 and 5. The values for m_e, m_h, v_l, c_s, ρ and ε_r are taken from [1–4]. E_d was taken from [22]. For $C_{\exp}$ see text

Parameter	Unit	Value of the parameter	
		Kr	Xe
Effective electron mass, m_e	m_0	0.42	0.35
Effective hole mass, m_h	m_0	3.6	2.1
Initial carrier density, N_0*	$1/m^3$	$3.6 \cdot 10^{14}$	$6 \cdot 10^{16}$
Initial excess energy, E_{excess}	meV	780	1450
Deformation potential, E_d	eV	not needed	0.79
$C_{\exp} = E_d^2 m_e^{5/2}$	$J^2 \cdot kg^{5/2}$	$4.83 \cdot 10^{-114}$	not used
Longitudinal sound velocity, v_l	m/s	1370***	not needed
Averaged sound velocity, c_s	m/s		830****
Crystal temperature, T_L	K	5.5	
Nonradiative losses, $\Gamma_{nr} = 1/\tau_{nr}$	1/s	0**	0**
Density of solid Kr at 5 K, ρ	kg/m^3	3092.6	3781
Relative dielectric permeability, ε_r		1.88	2.22

*The values were obtained neglecting the correction pointed out to us by A.N. Vasil'ev (see footnote 1). Including the correction means, the values have to be multiplied by a factor $(4\pi)^3$.

**If the value of nonradiative losses is smaller than $\approx 5 \cdot 10^7 s^{-1}$, its influence on the fits can be neglected.

***In the case of Kr, for the whole calculation, the longitudinal sound velocity was used.

****For the Xe calculations, the averaged sound velocity was used.

the fitting parameter characterizes the distribution after hole-trapping.

2.1.2. Argon and neon. In the light RGS, free excitons are rapidly self-trapped. Therefore, the method used in the case of Kr and Xe to study thermalization and recombination of free carriers cannot be used. In the case of Ar, we succeeded in analyzing recombination with the luminescence of self-trapped excitons. The STE emission of Ar consists of a singlet and a triplet band [1–4]. The lifetime of the singlet emission is 1.8 ns [23]. The formation should therefore be observable in the decay curves of the singlet component.

The singlet and the triplet STE bands overlap spectrally, and the singlet contribution is much weaker than the triplet one. Therefore, at first a photon energy of luminescence had to be found to get an optimal singlet / triplet ratio and sufficiently high counting rates. The chosen photon energies were 9.76 and 10.21 eV (for comparison: maximum of the triplet STE band 9.72 eV, of the singlet band 9.83 eV [24]).

In Fig. 6, decay curves of the singlet luminescence are shown. Most of the photon energies of excitation are above the band gap energy, $E_g = 14.16$ eV. With increasing photon energy of excitation, up to a value $E_{\text{th}} = E_g + E_{\text{ex}}$ (which will be discussed below; E_{ex} is energy of the $n = 1$ exciton), the curves get more and more cascadelike. They were fitted with the sum of two exponentials,

$$I(t) = I_0 + A_1 \exp(-t/\tau_1) + A_2 \exp(-t/\tau_2) \quad (7)$$

(A_1, A_2 with opposite sign). The results of the fits (τ_1 and τ_2) are shown in Fig. 7 as a function of photon energy of excitation [24]. Apart from the range where the values of both time constants are comparable, the decay time is independent from photon energy of excitation*. This time corresponds to the lifetime of the

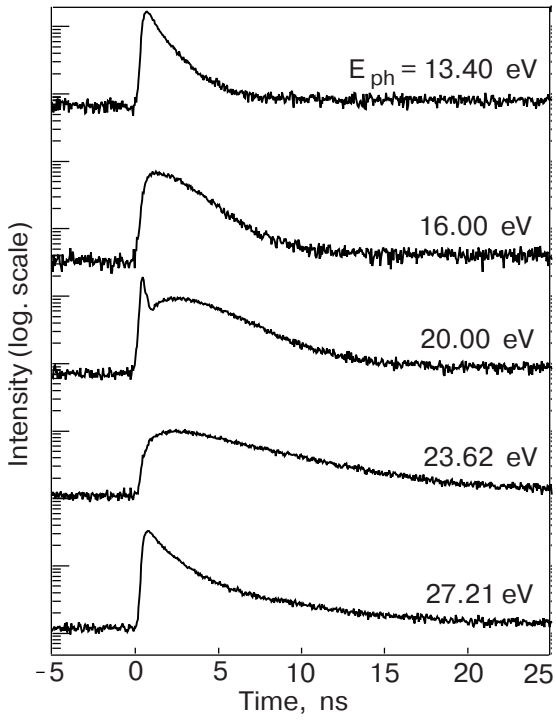

Fig. 6. Decay curves of the STE luminescence of Ar, measured at $T = 8$ K at a luminescence photon energy 10.21 eV [24]. The resolution intervals are $\Delta\lambda = 1.75$ Å in excitation and $\Delta\lambda = 11$ Å in emission. The photon energy of excitation is given at each curve.

* For mathematical reasons, the accuracy of the fits is lower for nearly equal time constans $\tau_1 \approx \tau_2$.

STE singlet, and the value is in good agreement with the one reported by Roick et al. [23]. The rise times for excitation below the band gap correspond to the experimental time resolution. For excitation above the band gap, we observe a linear increase of the rise time until it reaches the value of the lifetime of the singlet state*. Above E_{th}, the rise time drops to the value it has in the excitonic range of excitation. There, the decay curves are nearly identical with those observed under excitation with a photon energy below the band-gap energy (see Fig. 6).

In view of Sec. 2.1.1, the increase of the rise time is ascribed to the thermalization of the electrons. From the slope of the linear increase of τ_2, a loss rate of approximately 5 eV/ns (slope of the straight line: 0.2 ns/eV) is obtained. With an average phonon energy 5 meV this corresponds to a loss of one phonon energy per one ps, in other words, an average scattering rate of 10^{12} s^{-1} has been observed.

Concerning Ne, systematic measurements like in the case of Ar were not possible up to now due to experimental difficulties.

2.2. Time-resolved excitation spectra and «prompt» secondary exciton formation

2.2.1. FE line of Kr *and* Xe. Under pulsed excitation with a sufficiently large interpulse period, the recombination-type luminescence at $t = 0$ (defined by the excitation pulse) starts from zero. On the other hand, excitons created at $t = 0$ start emitting at $t = 0$ with maximum intensity. Based on these ideas, time-resolved excitation spectra can be used to discriminate between «prompt» (within the experimental time resolution) secondary excitons and delayed recombination-type secondary excitons. In a time-resolved excitation spectrum, following pulsed excitation, the luminescence intensity is measured within a time-interval (called time-window) of length Δt with a delay δt with respect to the exciting pulse. Without delay and with a short time-window, we are sensitive for prompt secondary excitons. With a delay much larger than the lifetime of prompt excitons, we are sensitive for recombination-type excitons. If the delay is zero, the time-window accepts scattered light of the exciting light pulse. Therefore sometimes a slight delay is chosen to suppress scattered light, however at the expense of sensitivity for prompt luminescence. Some results have already been published [10,12,25–27].

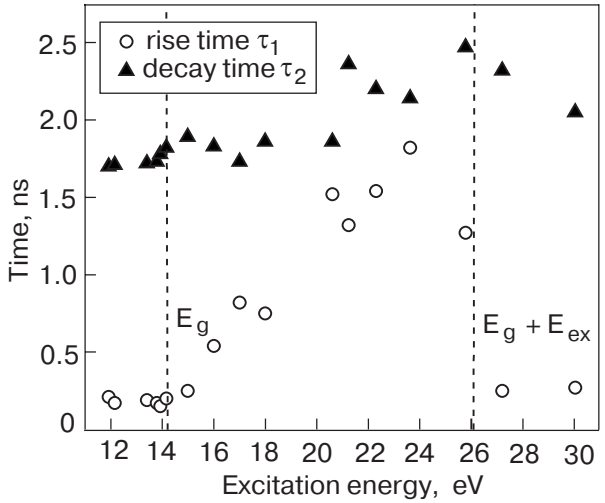

Fig. 7. Plot of the characteristic times of the cascade-type fits of decay curves of the STE singlet state of Ar as a function of photon energy of excitation [24]. The band gap at 14.15 eV and the threshold energy $E_{th} = E_g + E_{ex}$ are marked.

In Fig. 8, time-resolved excitation spectra of the FE line of Kr and Xe, measured in short time-windows are presented. The details of the time-windows are given in the figure caption. The special photon energy scale is well suited to illuminate the physics behind the phenomena observed. The unit of the scale is the exciton energy (Xe: 8.36 eV, Kr: 10.14 eV). As zero-point, the band-gap energy is chosen. In both curves, we observe (i) low intensity, until a threshold E_{th} at point 1 is reached, and (ii) a dramatic increase of intensity above E_{th}.

The low intensity underlines the slow formation of secondary excitons via recombination. The increase of the signal above the threshold underlines, that in this range of excitation, «prompt» secondary excitons are created. In Kr as well as in Xe, an analysis [10,12] of the threshold energy shows that it is given within ±0.2 eV by

$$E_{th} = E_g + E_{ex}. \qquad (8)$$

This is the energy required (from point of view of energy conservation) to obtain one electron-hole pair with negligible kinetic energy and one exciton. In both cases, the time-resolved excitation spectrum yields a broad maximum above E_{th}. It does not drop to the low value as on the low energy side but levels off. At higher photon energies, another increase is found, starting approximately at an energy $E_g + 2E_{ex}$.

There are two mechanisms for the prompt secondary exciton creation observed above threshold E_{th}, (i) inelastic scattering of photoelectrons at a valence electron resulting in an additional exciton, and (ii) *simultaneous* creation of an electron-hole pair and an exciton (electronic polaron complex [28]). Contrary to the electronic

* Of course, it is an accidental coincidence of both values.

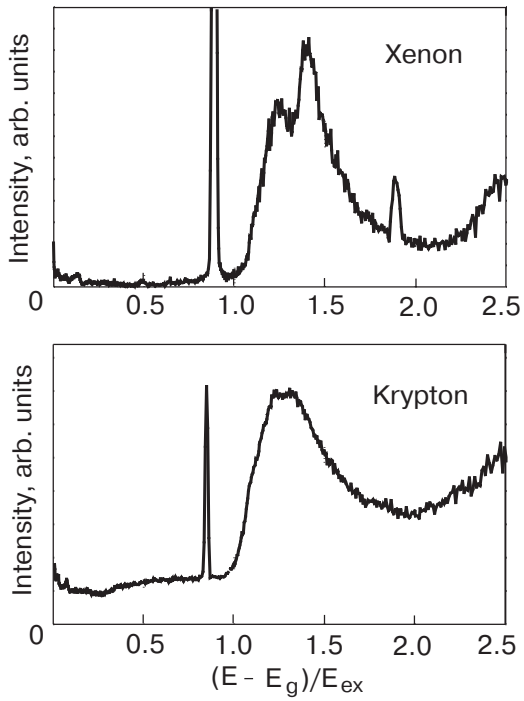

Fig. 8. Time-resolved excitation spectra of the FE luminescence of solid Kr [12] and Xe [30], plotted in an energy scale which is described in the text. The time windows and time delays are: $\Delta t = 0.94$ ns, $\delta t = 0$ ns (Kr); $\Delta t = 0.8$ ns, $\delta t = 0.6$ ns (Xe). The sharp maxima arise from scattered light.

polaron complex, the scattering mechanism is a *sequential* process. The scattering time in the fs regime cannot be resolved in our experiments, therefore, these secondary excitons are called prompt as well. On the other hand, excitons created simultaneously with an electron-hole pair could also be called «direct» because they are the result of a primary excitation process.

From an experimental point of view it is difficult to discriminate between both mechanisms. At first, it was pointed out that a discrimination should be possible via the threshold energy because the simplest scattering model predicts a threshold considerably larger than the one predicted for the electronic polaron complex [10]. The simple model assumes parabolic bands, neglecting Bragg reflection across the Brillouin zone boundaries. With the so-called mutiple-parabolic-branch-band (MPPB) model by Vasil'ev et al. [29] it was shown that the threshold is practically the same for both mechanisms [12,30]. An argument in favour of the electronic polaron complex is the fact that theory predicts a resonance as it is observed, whereas the scattering process leads to a more stepwise increase of the excitation spectrum. Summing up, the curves are ascribed to inelastic scattering with a resonant enhancement near threshold due to the formation of electronic polaron complexes. In a certain sense, the time-resolved excitation spectra bring about excitonic sidebands of valence ionization as they were predicted by theory, $E_{\rm res} = E_g + nE_{\rm ex}$, n is integer [28].

2.2.2. The special case of argon and neon. In the light RGS, FE luminescence is missing. Time-resolved (Ar) and time-integrated (Ne) excitation spectra of the STE emission, however, yield similar results as in the case of Xe and Kr. The drop of the rise time τ_2 (see Fig. 7) around $E_{\rm th}$ also shows that above $E_{\rm th}$ prompt secondary excitons are created. In Figs. 9 and 10, data are presented for Ar [24,31] and Ne [24]. In the case of Ar, the singlet component of the STE has been chosen as a fast decay channel for *time-resolved* excitation spectra (observation at 10.21 eV), in the case of Ne, the emissions of the atomic-type STE at 16.75 eV and of the so-called W-band at 15.5 eV were used for *time-integrated* measurements. Nevertheless, the threshold of prompt secondary exciton creation at $E_{\rm th} = E_g + E_{\rm ex}$ was observed. In the case of Ar, a broad resonance like in the heavy rare gases shows up, in the case of Ne (time-integrated spectrum), a more step-like increase was found. It has to be admitted that the spectral range of the Ne-measurements is unfavorable for both beamlines used. The interesting features are close to the limits of the working ranges of the respective monochromators (left part of Fig. 10: normal-incidence monochromator, right part of Fig. 10: grazing-incidence monochromator) where the excitation intensity is small. The threshold itself and the creation of prompt secondary excitons is well established.

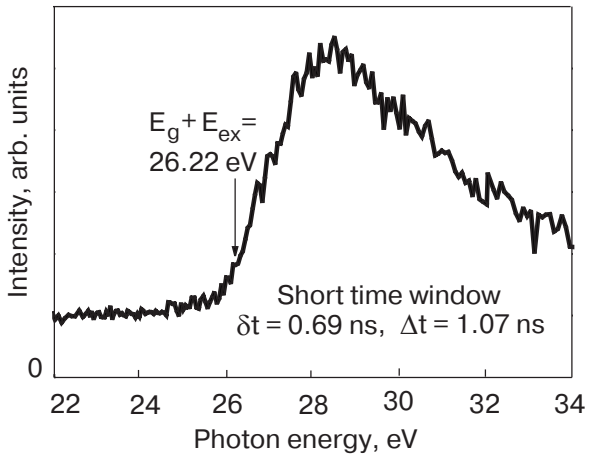

Fig. 9. Time-resolved excitation spectrum of STE luminescence of Ar [24,31]. Due to the photon energy of observation chosen (10.21 eV), the main contribution in the time window $\Delta t = 1.07$ ns and $\delta t = 0.69$ ns arises from the singlet STE. $T = 8$ K. Resolution intervals as in Fig. 6.

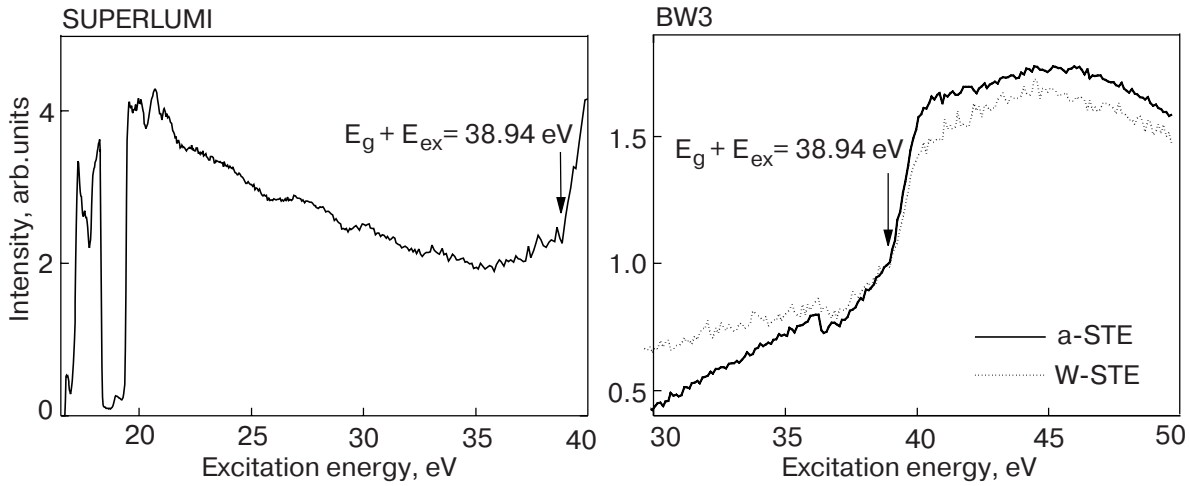

Fig. 10. Time-integrated luminescence excitation spectra of Ne [24]. Left part measured at the SUPERLUMI station (normal incidence range) at 16.75 eV (atomic-type STE). The curves in the right part were measured at the undulator beamline BW3 at 16.4 eV (a-STE) and at 15.5 eV (W-band). T = 6 K. The resolution interval in excitation was 0.01 eV (a-STE) and 0.02 eV (W-band).

3. Secondary excitons following inner-shell excitation

3.1. Excitonic sidebands of inner shell ionization limits

Here, we start with a presentation of time-resolved excitation spectra of FE luminescence in the vicinity of the Kr 3*d* and Xe 4*d* inner-shell excitation (Fig. 11 [34]). The (spin-orbit split) ionization energies are Kr $3d_{5/2}$: 92.32 eV, Kr $3d_{3/2}$: 93.50 eV; Xe $4d_{5/2}$: 65.59 eV, Xe $4d_{3/2}$: 67.54 eV (averages of the values given by Resca et al. [32] and Kassühlke [33]). For comparison purposes, the spectra are aligned for the respective $d_{5/2}$ ionization limits, and the spread of the scales corresponds to the respective exciton energies (vertical lines). The numbers given at the abscissa, however, are electron-volts. Similar to the valence case, strong resonances with a threshold energy $E_{\rm th} = E_{d_{5/2}} + E_{\rm ex}$ are observed. In the case of Xe, the resonance is split. The second peak is ascribed to a resonance with a threshold $E_{d_{3/2}} + E_{\rm ex}$. Experiments with higher spectral resolution show that the Kr resonance also contains two contributions, one of them being correlated to the $d_{3/2}$ ionization limit*. Moreover, a second resonance with a threshold $E_{\rm th} = E_{d_{5/2}} + 2E_{\rm ex}$ is observed. In conclusion, excitonic side bands exist not only in the range of valence excitations but also in the range of inner-shell excitations.

In the case of light rare gas solids, up to now only the Ar 2*p* excitations have been investigated [24,35]. The results yield an excitonic sideband as well, however, degradation of the samples due to radiation damage is severe, therefore the excitation spectra suffer from an overall decrease of intensity during the measurements.

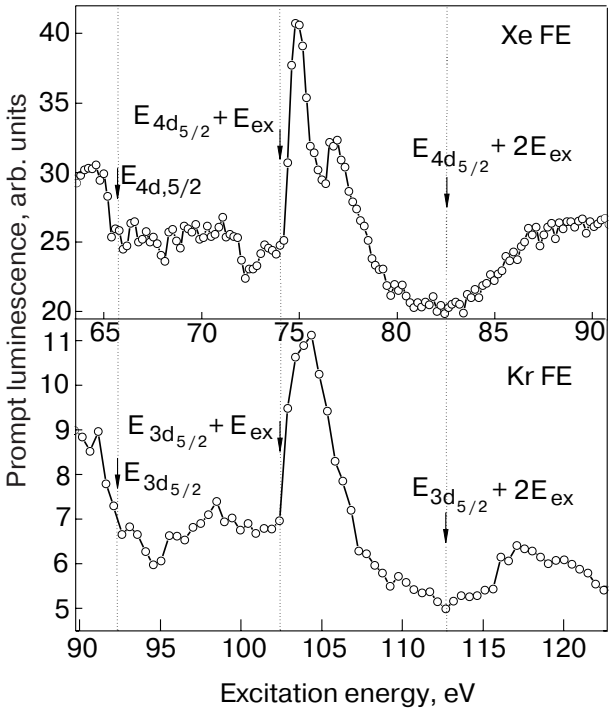

Fig. 11. Time-resolved excitation spectra of FE luminescence of Kr and Xe in the vicinity of the Kr 3*d* and the Xe 4*d* inner shell excitations [34]. The time windows are Kr: Δt = 1.6 ns, δt = 0; Xe: Δt = 1.2 ns, δt = 0. For details, especially for the scale used, see text.

* In Fig. 11 we preferred to present a quick scan. During high-resolution scans, which take some hours, the samples degrade due to defect formation. This leads to a continuous decrease of FE luminescence. High-resolution scans are given in [34].

4. Carrier recombination and density effects

The influence of inner-shell excitation on the decay curves is illustrated in Fig. 12 with a set of decay curves of the FE line of Xe, presented as a function of time and photon energy of excitation around the excitonic sideband of $4d_{5/2}$ ionisation. Prompt and delayed FE luminescence is observed [36]. As soon as the photon energy of excitation crosses the threshold of the excitonic sideband, the prompt part increases at the expense of the delayed part, indicating a redistribution among prompt and delayed secondary excitons. The prompt part below threshold originates from inelastic scattering of photoelectrons originating from valence excitations. The superposition of valence and inner-shell excitations makes a quantitative analysis difficult. Therefore, we restrict ourselves to present these qualitative results.

Excitation in the same range of excitation made feasible another type of investigation. The measurements have been carried out at the undulator beamline BW3 of HASYLAB with its high excitation intensity [37]. By tuning the undulator gap the spectral position of the first harmonic is tuned. With fixed settings of photon energy, it means that the intensity is tuned across the first harmonic. In this way, the excitation density can be varied by a factor of 50. This was used to establish density effects in the carrier dynamics. The models used to analyze the delayed FE decay predict such effects (Eq. (4)). An excitation below the thresholds of the sidebands was chosen to avoid interference with the strong contribution of prompt secondary excitons originating from the sideband.

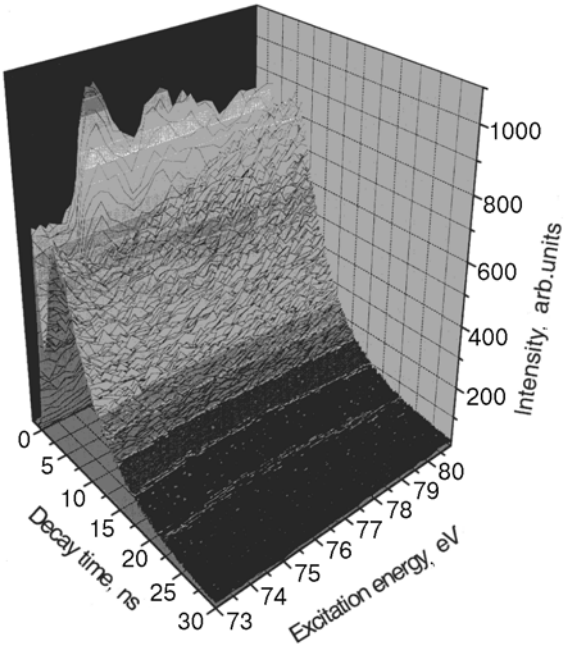

Fig. 12. Set of decay curves of the FE luminescence of Xe in the vicinity of the excitonic sideband of $5d_{5/2}$ ionization [36]. For details see text.

In Fig. 13, decay curves of the FE lines of Kr (excitation 85.3 eV) and Xe (excitation 66.1 eV) are presented [38]. The parameter of the curves is the initial carrier density at $t = 0$, obtained from the fits. With increasing carrier density, the delayed part of the decay curves changes. The maximum shifts to smaller times. The full curves are fits with equations (3)–(5). The variation of the excitation density by a factor of 50 leads to relatively small changes in the shape of the decay curves, although the product of the initial carrier densities in the rate Eq. (4) varies by a factor of 2500. This is explained by the fast increase of the recombination cross-section $\sigma(T_e)$ (Eq. (5)) within the first nanoseconds [15], which strongly influences the shape of the decay curves independently from the carrier densities.

Concerning the parameters, the situation is more complex than in the case of excitations into states near to the bottom of the conduction band. The initial kinetic energy of the photoelectrons (we still assume fast hole relaxation to the top of the valence band) is an open question because a broad distribution as a consequence of inelastic scattering of the *initially* created photoelectrons is expected. The time scale for this redistribution is far below the experimental time resolution. Therefore, a mean kinetic energy of the electrons after redistribution, E_0, was introduced as a fit parameter to replace the well-defined energy for valence excitations, E_0, of Eq. (2).

It turned out that the nonradiative channel in the rate equations can not be neglected. The nonradiative rate, $1/\tau_{nr}$ has a more phenomenological character and strongly depends on sample conditions. As in the case of valence excitations, the initial carrier densities $n_{e0} = n_{h0}$ (after the fast redistributions due to elastic and inelastic scattering) have to be included as fitting parameters. They were introduced with the constraint that they are proportional to the measured excitation density. As three fitting parameters were unavoidable, a fourth one, namely the effective mass of the electrons, was tolerated. Values are given in Table 3 [36,38].

The m_e values are within reasonable limits, but cannot be taken as definite, since they are coupled to E_d in the model via $E_d^2\, m_e^{5/2}$. The E_0-values seem to be in contradiction to photoemission data which show that the bulk of the photoelectrons have kinetic energies between zero and 2 eV in the range of Xe 4*d* and Kr 3*d* excitation [33]. Note, however, the electrons below the vacuum level are not observed in photoemission. E_0 obviously does not correspond to the mean kinetic energy after redistribution via electron-electron scattering as it is observed in photoemission. It is ascribed to that

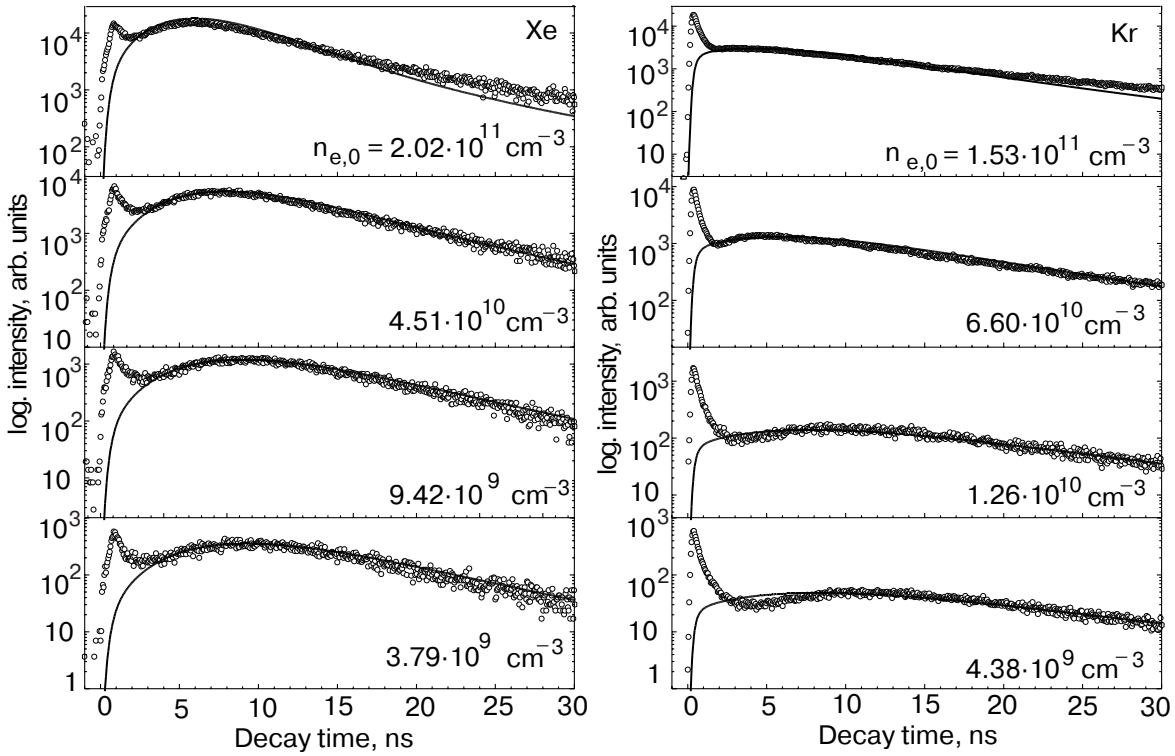

Fig. 13. Decay curves of the FE luminescence of Kr and Xe, measured with different excitation densities (circles), together with fitting results for the delayed part (full curves) [38]. The initial electron densities for the calculations are given at each curve, the other fit parameters are given in Table 3. The Kr curves were measured for 85.3 eV excitation at 12.5 K, the Xe curves were measured at 66.1 eV excitation at 10.8 eV.

Table 3

The values of the parameters used for the fits of delayed FE luminescence in solid Kr and Xe shown in Fig. 13. The values of m_e, $n_{e,0}$, E_0, and τ_{nr} are fit-results. m_k, v_l, c_s, ρ, and ε_r are taken from [1–4]. E_d of Kr was calculated from the low field mobility [21] with the literature value of the effective electron mass given in Table 2. E_d of Xe was taken from [22]

Parameter	Unit	Value of the parameter	
		Kr	Xe
Effective electron mass, m_e	m_0	0.36	0.73
Effective hole mass, m_h	m_0	3.6	2.1
Initial carrier density, $n_{e,0}$	$1/m^3$	$1.53 \cdot 10^{17}$	$2.02 \cdot 10^{17}$
Mean electron energy, E_0	meV	56	24
Deformation potential, E_d	eV	1.44	0.79
Longitudinal sound velocity, v_l	m/s	1370	1300
Averaged sound velocity, c_s	m/s	845	830
Crystal temperature, T_L	K	12.5	10.8
Nonradiative losses, $\Gamma_{nr} = 1/\tau_{nr}$	1/s	$1/25.9 \cdot 10^{-9}$	$1/13.1 \cdot 10^{-9}$
Density of solid Kr at 5K, ρ	kg/m^3	3092.6	3781
Relative dielectric permeability, ε_r		1.88	2.22

range of kinetic energy, in which the rates for electron-hole recombination and further phonon-relaxation get comparable. An estimate for the *excitation density* based on absolute flux measurements is about two orders of magnitude higher than the results of the fits. This discrepancy corresponds to the small values of E_0 insofar as diffusion processes during the first stage of relaxation to E_0 may considerably reduce the density. Although significant simplifications have been applied, both for Kr and Xe the whole set of data can be described with a reasonable and consistent set of parameter values.

Conclusions

It was shown that time-resolved luminescence spectroscopy on rare gas solids is a powerful tool to investigate the dynamics of photocarriers, namely electronic relaxation, thermalization and recombination into secondary excitons. The time-evolution of free excitons following primary valence excitation and to a certain extend also following inner-shell excitation can be explained in terms of the «classical» theory of the relaxation processes mentioned, with values of the various physical quantities involved, as they are reported in the literature. One of the main results is the proof that there exist excitonic sidebands of ionization

limits (either band gap or inner shell ionization) which are ascribed to electronic polaron complexes. Due to the fact that thermalization is slow in rare gas solids, a moderate time resolution is sufficient to carry out the experiments.

Acknowledgments

The work was supported by the Bundesministerium für Bildung und Forschung (grants No. 05 650GUB, 05 ST8GUI 6) and by the Deutsche Forschungsgemeinschaft DFG (grants No. DFG Zi 159/1-4). V. Kisand and G. Zimmerer acknowledge support by the EU — Project «Regional Centre of Excellence in New Functional Materials, their Design, Diagnostics and Exploitation» (No. ICA1-1999-70086).

1. I.Ya. Fugol', *Adv. Physics* **27**, 1 (1978); *ibid*. **37,** 1 (1988).
2. N. Schwentner, E.E. Koch, and J. Jortner, *Electronic Excitations in Condensed Rare Gases*, *Springer Tracts in Modern Physics*, **107,** Springer-Verlag, Berlin, Heidelberg (1985).
3. V. Saile, *Appl. Optics* **19,** 4115 (1980).
4. G. Zimmerer, in: *Excited State Spectroscopy in Solids*, U.M. Grassano and N. Terzi (eds.), North Holland Publishing, Amsterdam (1987), p. 37.
5. U. Rössler, in: *Rare Gas Solids*, M.N. Klein and J. A. Venables (eds.), **1**, Academic Press London, New York, San Francisco (1976/77), p. 505.
6. F. Coletti, *Thèse d'Etat*, Université Aix-Marseille II, (1987).
7. T. Kloiber, *Dissertation*, The University of Hamburg (1989).
8. R. Kink and M. Selg, *Phys. Status Solidi* **B96** 101 (1979).
9. V. Kisand, M. Kirm, S. Vielhauer, and G. Zimmerer, *J. Phys.: Condens. Matter* **14**, 5529 (2002).
10. B. Steeg, M. Kirm, V. Kisand, S. Körding, S. Vielhauer, and G. Zimmerer, *J. Low Temp. Phys.* **111,** 739 (1998).
11. G. Baldini, *Phys. Rev.* **128**, 1562 (1962).
12. V. Kisand, M. Kirm, E. Negodin, E. Sombrowski, B. Steeg, S. Vielhauer, and G. Zimmerer, *J. Phys.*: *Condens. Matter* **15**, 2023 (2003).
13. D. Varding, I. Reimand, and G. Zimmerer, *Phys. Status Solidi* **B185**, 301 **(1994).**
14. D. Varding, J. Becker, L. Frankenstein, B. Peters, M. Runner, A. Schröder, and G. Zimmerer, *Fiz. Nizk. Temp.* **19**, 600 (1993) [*Low Temp. Phys.* **19**, 427 (1993)].
15. I. Reimand, E. Gminder, M. Kirm, V. Kisand, B. Steeg, D. Varding, and G. Zimmerer, *Phys. Status Solidi* **B214**, 81 (1999).
16 V. Kisand, M. Kirm, S. Vielhauer, and G. Zimmerer, *Sur. Rev. Lett.* **9**, 783 (2002).
17. E.M. Conwell, *High Field Transport in Semiconductors*, vol. **9**, Solid State Physics Academic Press, New York and London (1967).
18. A.N. Vasil'ev, Moscow State University, Physics Department, private communication.
19. V.N. Abakumov, V.I. Perel', and I.N. Yassievich, *Sov. Phys. JETP* **51**, 626 (1980).
20. J.M. Ziman, *Electrons and Phonons: The Theory of Transport Phenomena in Solids*, Clarendon (1962).
21. L.S. Miller, S. Howe, and W.E. Spear, *Phys. Rev.* **166**, 871 (1968).
22. A.M. Ratner, *Phys. Rep.* **269**, 197 (1996).
23. E. Roick, R. Gaethke, P. Gürtler, T.O. Woodruff, and G. Zimmerer, *J. Phys.* **C17**, 945 (1984).
24. E. Gminder, *Dissertation*, The University of Hamburg (2000).
25. B. Steeg, E. Gminder, M. Kirm, V. Kisand, S. Vielhauer, and G. Zimmerer, *J. Electr. Spectr. Rel. Phenomena* **101–103**, 879 (1999).
26. V. Kisand, *Proc. 3rd Internat. Conf. on Excitonic Processes in Condensed Matter EXCON'98*, R.T. Williams and W.M. Yen (eds.), The Electrochem. Soc., INC., Pennington, NJ, USA, Proceedings Volume **98–25**, p. 385.
27. V. Kisand, E. Gminder, M. Kirm, B. Steeg, S. Vielhauer and G. Zimmerer, *Proc. 5th Inter. Conf. on Inorganic Scintillators and Their Applications*, August 16–20, 1999, V.V. Mikhailin (ed.), Moscow, Faculty of Physics, M.V. Lomonosov Moscow State University (2000), p. 458.
28. J.T. Devreese, A.B. Kunz, and T.C. Collins, *Solid State Commun.* **11**, 673 (1972).
29. A.N. Vasil'ev, Y. Fang, and V.V. Mikhailin, *Phys. Rev.* **B60**, 5340 (1999).
30. B. Steeg, *Dissertation*, The University of Hamburg (1999).
31. E. Gminder, M. Kirm, V. Kisand, B. Steeg, S. Vielhauer, and G. Zimmerer, *J. Luminescence* **87–89**, 555 (2000).
32. L. Resca, R. Resta, and S. Rodriguez, *Phys. Rev.* **B18**, 702 (1978).
33. B. Kassühlke, *Dissertation*, TU München (1998).
34. S. Vielhauer, E. Gminder, M. Kirm, V. Kisand, E. Negodin, B. Steeg, and G. Zimmerer, *Int. J. Modern Physics* **B15**, 3695 (2001).
35. S. Vielhauer, M. Kirm, V. Kisand, E. Negodin, E. Sombrowski, B. Steeg, and G. Zimmerer, *Surf. Rev. Lett.* **9**, 1333 (2002).
36. S. Vielhauer, *Dissertation*, The University of Hamburg (2003).
37. T. Möller, *Synchr. Rad. News* **6**, 16 (1993).
38. S. Vielhauer, M. Kirm, V. Kisand, B. Steeg, A.N. Vasil'ev, and G. Zimmerer, *J. Nonlinear Optics* **29**, 315 (2003).